Quaternary Geochronology 4 (2009) 525–532

Contents lists available at ScienceDirect

Quaternary Geochronology

journal homepage: www.elsevier.com/locate/quageo

Research Paper

Cosmogenic ^{3}He exposure ages and geochemistry of basalts from Ascension Island, Atlantic Ocean

K. Ammon [a,*], T.J. Dunai [a], F.M. Stuart [b], A.-S. Meriaux [a,c], E. Gayer [a,d]

[a] School of GeoSciences, University of Edinburgh, Drummond Street, Edinburgh EH8 9XP, United Kingdom
[b] Isotope Geosciences Unit, Scottish Universities Environmental Research Centre, East Kilbride, United Kingdom
[c] School of Geography, Politics, and Sociology, Newcastle University, United Kingdom
[d] Institut de Physique du Globe de Paris, Paris, France

ARTICLE INFO

Article history:
Received 25 February 2009
Received in revised form
3 September 2009
Accepted 4 September 2009
Available online 12 September 2009

Keywords:
^{3}He exposure ages
Eruptive history of Ascension Island
Magmatic ^{3}He/^{4}He ratio

ABSTRACT

The chronology and origin of volcanism of Ascension Island, South Atlantic Ocean, is poorly resolved. Here we use *in situ* produced cosmogenic ^{3}He in olivine and pyroxene phenocrysts from well-preserved lava flows to date the main sub-aerial basalt volcanism on the island. Etching olivine separates in HF/HNO_3 appears to remove a significant proportion of the implanted radiogenic ^{4}He contribution. Average exposure ages of each flow corrected for radiogenic He range from 328 ka to 186 ka and are used to refine the chronology and stratigraphy of the island. Magmatic ^{3}He/^{4}He ratios derived from *in vacuo* crushing are in the range of 6.3–7.3 R_A. This range is lower than the neighbouring Mid-Atlantic Ridge segment (6–8°S) but slightly higher than measured in regional ocean islands of St. Helena, Tristan da Cunha and Gough. Combining these data with new trace element data and published radiogenic isotope ratios it appears that the Ascension Island magmatism is a mix of HIMU mantle material, typified by basalts from St. Helena, and depleted MORB-source mantle.

1. Introduction

Ascension Island is the emergent top of a volcano situated at 7°56′S and 14°22′W in the South Atlantic Ocean, approximately 90 km west of the Mid-Atlantic Ridge and 50 km south of the Ascension Fracture Zone (e.g., Bourdon and Hemond, 2001; Nielson and Sibbett, 1996). It rises about 860 m above sea level and the base of the volcano covers about 2000 km^2 approximately 3200 m beneath sea level (Weaver et al., 1996). Volcanic rocks from Ascension Island span a compositional sequence from transitional to mildly-alkaline basalt to rhyolite. Volcanic activity probably started at 6–7 Ma (Klingelhoefer et al., 2001). The oldest trachytic intrusions on the island are 0.6–1.0 Ma (Weaver et al., 1996 and refs. therein). However, the basaltic volcanism on the island has not been dated reliably and consequently the recent eruptive history of Ascension Island is poorly constrained.

Dating young basalts is often hindered by the absence of suitable materials for the different dating methods (e.g., Laughlin et al., 1994). Dating young basalts (less than a few 100 kyr) by ^{40}Ar–^{39}Ar or K–Ar requires high K concentrations and is frequently limited by the presence of "excess" ^{40}Ar and high concentrations of air-derived Ar in groundmass glass and altered minerals. *In situ* produced cosmogenic ^{3}He is well suited to dating Plio-Pleistocene basaltic flows because the production rate in olivine and pyroxene phenocrysts is high enough to produce measurable ^{3}He concentrations in a few thousand years of exposure (e.g., Gosse and Phillips, 2001; Kurz et al., 1990).

Here we use cosmogenic ^{3}He in olivine and pyroxene phenocrysts from lava flow surfaces to determine the eruption phases of the main basaltic rock types on Ascension Island. In addition we use the ^{3}He/^{4}He ratio of magmatic volatiles trapped in the phenocrysts, along with trace element analyses of the basalts themselves, to draw conclusions about the nature of the mantle beneath Ascension Island.

2. Geology of Ascension Island

Ascension Island is the result of off-axis melting anomalies in the sub-Atlantic Ocean mantle. There is little consensus about its origin, particularly whether it is related to upwelling beneath the nearby Mid-Atlantic Ridge or to a discrete mantle plume (Bourdon and Hemond, 2001; Brozena, 1986). Ascension Island is aligned with two un-named seamounts (termed A and B in Fig. 1) 300 and 610 km to the west, parallel to the Ascension Fracture Zone (AFZ) (Fig. 1). This is not consistent with a classic track of a fixed hotspot

* Corresponding author.
E-mail address: kammon@staffmail.ed.ac.uk (K. Ammon).

1871-1014/$ – see front matter Crown Copyright © 2009 Published by Elsevier B.V. All rights reserved.
doi:10.1016/j.quageo.2009.09.003

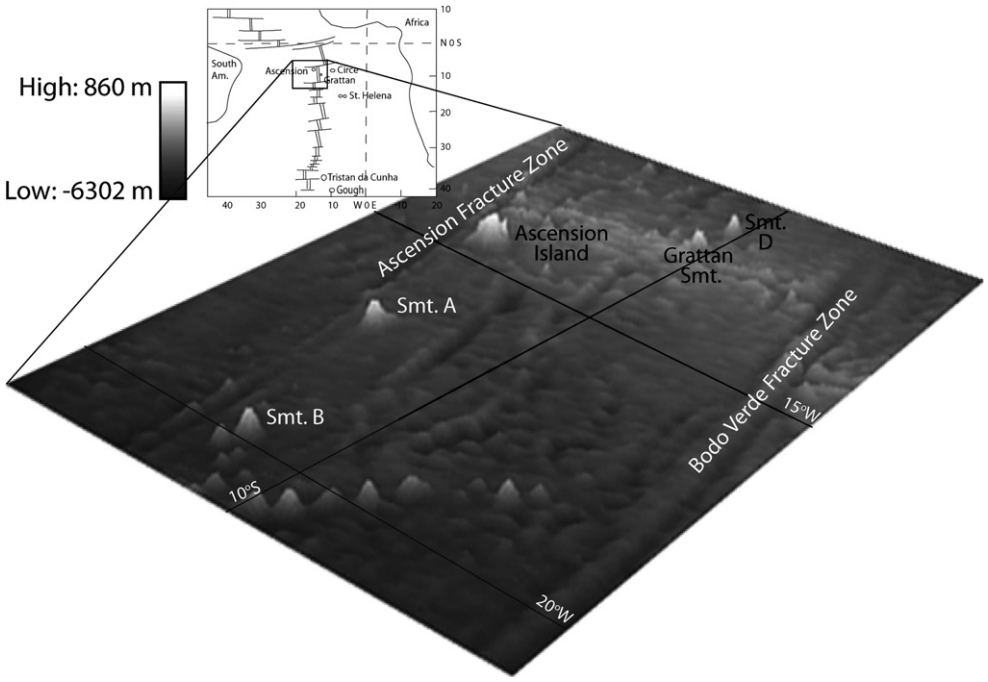

Fig. 1. Bathymetry data show the alignment of seamounts A, B, and Ascension Island (Picture is reproduced from the GEBCO One Minute Grid, version 2.0, http://www.gebco.net with kind permission of the British Oceanographic Data Centre (BODC)).

under the moving lithosphere. However, the shallow depth (positive depth anomaly), the missing rift valley, and the lack of seismicity suggests that a hotspot has passed beneath the ridge (Brozena, 1986). From the Pb isotopic composition of the nearby seafloor Bourdon and Hemond (2001) have proposed that the hotspot is currently located beneath the Grattan seamount (Fig. 1). Excess melt from a mantle plume could be channelled northwards through the ridge and stopped by the AFZ to build seamount A and Ascension Island (Brozena, 1986). This model could explain the volcanic eruptions subsequent to the major constructional phase on Ascension Island (Bourdon and Hemond, 2001) and therefore explain the young basaltic lava flows erupting after the older more developed trachytes. Minshull et al. (1998) proposed that Ascension Island and adjacent seamounts were built due to melting of ascending localised mantle heterogeneities.

The volcanic rocks on Ascension Island have a compositional range of basalt-hawaiite-mugearite-benmorite-trachyte-rhyolite (e.g., Nielson and Sibbett, 1996). This is understood to represent fractional crystallisation of alkali basalt magmas. A 3126 m long borehole samples almost the whole volcanic history of the island, and shows that the first erupted sub-marine lavas were basaltic in composition alternating with hyaloclastites (Nielson and Stiger, 1996). The oldest exposed sub-aerial eruptive centres on the island are felsic (Kar et al., 1998). The central felsic complex is exposed on the Middleton Ridge and the Green Mountain region (Fig. 2). Middleton Ridge is composed primarily of trachytic flows and pumice while Green Mountain is made up of massive pyroclastic deposits and trachyte (Kar et al., 1998). The eastern felsic complex is exposed in the area from the Devil's Caldron to the Letterbox (Fig. 2) and comprises trachyte flows and lava domes (Kar et al., 1998; Nielson and Sibbett, 1996). All these felsic lithologies are summarised as felsic flows and pyroclastic deposits in Fig. 2. Rhyolites from the central felsic complex have K–Ar ages ranging from 0.65 to 1.5 Ma (Harris et al., 1982; Nielson and Sibbett, 1996). Borehole samples yield ages of up to 3.6 Ma (Minshull et al., 2003). However, seismological investigations of the crustal structure reveal that Ascension Island could be much older than 3.6 Ma and volcanism could have started on-axis at 6–7 Ma (Klingelhoefer et al., 2001).

Subsequent volcanism is dominantly basaltic (Nielson and Sibbett, 1996). Four different basaltic magma types are distinguished (Weaver et al., 1996). Three of these basalt types are discriminated on the basis of distinct Zr/Nb ratios. The fourth type has an intermediate Zr/Nb but differs from the others by high-Ni/Zr and Sr/Zr (Weaver et al., 1996). The low-Zr/Nb basalts (4–4.5) are best represented by flows and scoria in the south-western part of the island. High-Zr/Nb basalts (5.5–6.0) are present in the south-eastern part of the island (Weaver et al., 1996). Basalts and hawaiite scoria cones and associated flows that cover the remainder of the island have

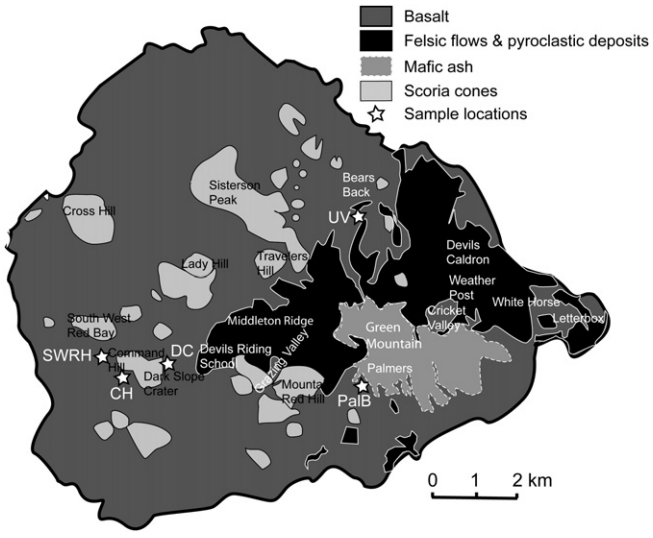

Fig. 2. Geology, topography and sampling locations on Ascension Island (Geological information is simplified from a map from Kar et al. (1998)).

intermediate Zr/Nb values (4.5–5.5) (Weaver et al., 1996). The high-Ni/Zr and high-Sr/Zr magma type is restricted to vents around Dark Slope Crater (Weaver et al., 1996).

On the basis of field observations Weaver et al. (1996) postulated that these different magma types do not overlap in time. The oldest basaltic lavas, the high-Zr/Nb-type (0.66 and 0.35 Ma; (Harris et al., 1982)), were followed by the eruption of the Dark Slope Crater (DSC) basalts. Subsequently low-Zr/Nb basalts were erupted during localised activity in the south of the DSC area. The final phase of volcanism is characterised by the widespread eruption of intermediate Zr/Nb lavas.

3. Samples and analytical technique

3.1. Sample sites

We have performed He isotope measurements on olivine and/or pyroxene phenocrysts from basalts from three of the main basalt suites that span almost the whole range of basaltic volcanism on the island (Fig. 2). High-Zr/Nb basalts were sampled on the southern flank of Green Mountain in the vicinity of Palmers. High-Ni/Zr basalts were taken from three sites in the vicinity of Dark Slope Crater and Command Hill. Intermediate -Zr/Nb basalts were sampled on the northeast of the island between Bears Back and Upper Valley Crater.

Samples were taken from three locations around Palmers along a distance of about 600 m (PalA, -B, and -C). At location PalB five samples were taken within an area of about 25 m^2. The uppermost 5 cm from pressure ridges were sampled for exposure dating. The flow is highly vesicular and thin-sections reveal the basalt contains large plagioclase phenocrysts (up to 2 mm) and less abundant smaller pyroxenes and olivines (100–500 μm). The flow appears to be slightly weathered (See pictures in Background dataset).

The three sample sites (DC: Dark Slope Crater, CH: Command Hill, SWRH: South West Bay Red Hill) (Fig. 2) in the Dark Slope Crater area lie within an area of less than 1 km^2. At each location five samples were taken within 5 m of each other. All flows have well-preserved surfaces, including intricate flow-top features (See pictures in Background dataset) Based on the preservation of these features we estimate that the total erosion of flow tops in this area is less than 1–2 cm. The uppermost 5 cm were sampled for exposure dating. The highly vesicular basalt flows are all rich in large (1–3 mm) plagioclase phenocrysts and smaller pyroxenes and olivines (mostly <1 mm).

Samples of fresh, highly vesicular plagioclase- and pyroxene-phyric basalts were taken from the Upper Valley Crater area (UV) (Fig. 2). The preservation of intricate flow-top features on the flow indicates less than 1 cm erosion at these sites. The six samples taken in the Upper Valley Crater are from an area of about 200 m^2. The uppermost 5 cm of a pressure ridge were sampled for exposure dating (See pictures in Background dataset). No indication for ash cover has been observed at any of the sample locations.

3.2. Sample preparation and He isotope analysis

Rocks were crushed sieved and olivine and pyroxene were separated using magnetic and heavy liquid separation. Mineral separates were cleaned in oxalic acid to remove adhering basalt and iddingsite rims (single-etched samples). The likelihood that radiogenic ^{4}He produced in the basalt groundmass has been implanted into the phenocrysts was the motivation to etch several olivine samples with HF and HNO_3 in order to remove ~30% of sample mass (double-etched samples). This ensures that the outer parts of the grains that could contain implanted ^{4}He from the decay of U and Th in the surrounding groundmass are removed (U and Th data see Table 1). In Table 2 we distinguish between the double-etched (de) and the single-etched (se) samples. All mineral separates were then hand-picked under a binocular microscope.

Olivine and pyroxene were crushed *in vacuo* in a hydraulic multi-sample crusher. Where there was insufficient sample for crushing, phenocryst fractions of samples from the same flow were combined for the determination of the magmatic ^{3}He/^{4}He. To extract the lattice-hosted helium, samples were melted during two 20–30 min steps using a 808 nm diode laser (see Foeken et al., 2006). The second melting step typically released ≤ 5% of total and was performed to ensure total degassing. Complete coupling of the laser beam with olivine required the addition of degassed pyroxene powder. After melting the released gas underwent a short cleaning and the isotopic composition of He was measured on a MAP 215-50 noble gas mass spectrometer (Williams et al., 2005). Blanks were measured daily using the same procedure as for the samples. Blanks ranged from 0.8 to 4.0×10^{-17} cm^3 STP for ^{3}He and $1.5–3.4 \times 10^{-12}$ cm^3 STP for ^{4}He which is typically ≤1% of samples.

3.3. Whole rock and mineral chemistry analyses

Major and trace elements of whole rock samples (Tables 3 and 4) were analysed on a Panalytical PW2404 wavelength-dispersive sequential X-ray spectrometer at the School of GeoSciences, University of Edinburgh. Major element concentrations were measured on fused glass discs. Glass pellets were produced using ~0.9 g of powder mixed with a borate flux in a ratio of 1:5 (sample/flux). This mixture was fused in a Pt–Au crucible at 1100 °C. To determine the LOI (Loss on ignition) samples were preheated at 400 °C in a porcelain crucible prior to fusion. Trace element concentrations were measured on ~8 g pressed powder pellets.

The chemistry for olivines and pyroxenes was determined on an electron microprobe CAMECA SX100 at the School of GeoSciences, University of Edinburgh. Routine detection limits are in the order of 0.009–0.05 wt%. Uranium and thorium concentrations of representative whole rock samples have been measured by instrumental neutron activation analysis (INAA) at the Actlabs Activation Laboratories in Ontario, Canada.

4. Results and discussion

4.1. Determining cosmogenic ^{3}He concentrations

Helium in phenocrysts from basalts with low U and Th concentrations is derived from two sources. Cosmogenic ^{3}He produced in the mineral lattice and nearby groundmass and magmatic He which is trapped in melt/volatile inclusions that were trapped as the phenocryst grew in the magma system. The magmatic He is released by *in vacuo* crushing. Recent studies have shown that some crushing procedures result in the release of a significant amount of cosmogenic He if fine powder is produced (grain size <140 μm) (e.g., Blard et al., 2006 and refs therein). However, the SUERC crush procedure does not significantly heat samples and *in situ* cosmogenic He has never been observed in the crush gas fraction (e.g., Foeken et al., 2009). The cosmogenic He

Table 1
U and Th from bulk rock (ppm).

Sample name	U	Th
DC-2	<0.2	1.7
CH-2	<0.2	1.7
SWRH	0.5	1.5
PAL-B1	0.4	2.7
UV-1	1.8	6.8

Table 2
Cosmogenic ^{3}He data and exposure ages for pyroxene and olivine from Ascension Island basalts. All uncertainties are 1σ.

Sample	Mineral	Etch	Coordinates	Elevation [m]	Mass [mg]	*R*-factor	^{3}He/^{4}He R/R$_A$ ± 1σ		^{4}He [10^{-8} cm^3 STP/g] ± 1σ	Exposure age [ka] ± 1σ
							Crush	Melt	Melt	
CH1	Olivine	de	7°57′40.7S	122	47.9	se: 0.952	6.27 ± 0.86	330 ± 5	0.122 ± 0.001	192 ± 10
CH2	Olivine	de	14°23′47.4 W	122	46.6	de: 0.991	7.30 ± 1.27	121 ± 4	0.335 ± 0.002	188 ± 12
CH3	Olivine	de		122	47.0			151 ± 3	0.299 ± 0.002	210 ± 12
CH3	Olivine	se		122	47.6			151 ± 5	0.275 ± 0.002	202 ± 12
CH4	Olivine	de		122	57.6			4.6 ± 0.14	8.976 ± 0.092	200 ± 12
CH5	Olivine	de		122	48.2			0.82 ± 0.03	53.78 ± 0.548	211 ± 13
CH1	Pyroxene	se		122	169.4	0.966	6.33 ± 6.47	551 ± 16	0.071 ± 0.002	194 ± 8
CH2	Pyroxene	se		122	34.5			45 ± 2	1.045 ± 0.013	200 ± 10
CH3	Pyroxene	se		122	108.8			288 ± 7	0.157 ± 0.003	222 ± 7
CH4	Pyroxene	se		122	99.4			415 ± 13	0.094 ± 0.004	193 ± 10
CH5	Pyroxene	se		122	61.6			402 ± 7	0.112 ± 0.003	223 ± 7
DC2	Olivine	de	7°57′31.7S	137	122.5	se: 0.952	6.80 ± 0.38	189 ± 10	0.209 ± 0.005	180 ± 12
DC3	Olivine	de	14°23′12.9 W	137	122.5	de: 0.991	7.08 ± 0.92	488 ± 18	0.077 ± 0.003	181 ± 12
DC3	Olivine	se		137	72.2			179 ± 6	0.199 ± 0.001	172 ± 11
DC3	Olivine	se		137	122.5			164 ± 4	0.236 ± 0.006	182 ± 10
DC4	Olivine	de		137	48.7			97 ± 4	0.457 ± 0.003	198 ± 13
DC5	Olivine	se		137	72.7			138 ± 6	0.284 ± 0.002	187 ± 12
DC5	Olivine	de		137	75.0			237 ± 6	0.173 ± 0.001	192 ± 11
DC1	Pyroxene	se		137	239.8	0.966		71 ± 1	0.517 ± 0.006	164 ± 4
DC2	Pyroxene	se		137	108.1			460 ± 15	0.080 ± 0.003	181 ± 9
DC3	Pyroxene	se		137	150.5			223 ± 4	0.170 ± 0.002	183 ± 5
DC4	Pyroxene	se		137	235.9			567 ± 16	0.078 ± 0.002	217 ± 8
DC5	Pyroxene	se		137	292.2			288 ± 5	0.138 ± 0.002	194 ± 5
SWRH1	Olivine	de	7°57′23.8S	107	55.0	0.985	6.99 ± 0.84	1.4 ± 0.05	33.98 ± 0.346	238 ± 14
SWRH4	Olivine	de	14°24′02.9 W	107	48.9			1.2 ± 0.03	44.98 ± 0.461	264 ± 15
PAL-B1	Pyroxene	se	7°57′46.8S	418	183.6	0.941	6.92 ± 0.77	149 ± 1	0.518 ± 0.004	293 ± 5
PAL-B1	Pyroxene	se	14°23′49.2 W	418	299.9			133 ± 2	0.568 ± 0.005	286 ± 7
PAL-B5	Pyroxene	se		418	274.9			179 ± 2	0.396 ± 0.003	270 ± 5
PAL-B5	Pyroxene	se		418	182.9			178 ± 3	0.434 ± 0.005	296 ± 6
UV1	Pyroxene	se	7°55′42.2S	155	107.7	0.805	6.61 ± 1.04	88 ± 2	0.725 ± 0.024	343 ± 13
UV1	Pyroxene	se	14°20′52.8 W	155	126.7		7.34 ± 2.04	84 ± 1	0.727 ± 0.006	325 ± 6
UV3	Pyroxene	se	7°55′44.7S 14°20′53.2 W	160	182.9			16 ± 0.3	6.108 ± 0.070	316 ± 19

de: double-etched samples and *se*: single-etched samples (see Section 3.2). Exposure ages include: radiogenic correction, magnetic field correction, self-shielding correction, and subsidence correction.

(^{3}He$_{cos}$) is calculated using the following equation (e.g., Kurz et al., 1990; Staudacher and Allegre, 1993):

$$^3\mathrm{He}_{cos} = {}^4\mathrm{He}_m \times (^3\mathrm{He}/^4\mathrm{He}_m - {}^3\mathrm{He}/^4\mathrm{He}_{cr}) \quad (1)$$

where ^{4}He$_m$ and ^{3}He/^{4}He$_m$ are the He concentration and isotopic ratio of the melt steps, and ^{3}He/^{4}He$_{cr}$ is the isotopic ratio of the magmatic He measured from the crush extraction.

For basalts with high U and Th concentration radiogenic ^{4}He, both produced *in situ* and implanted, can be significant in phenocrysts (Williams et al., 2005). Radiogenic ^{4}He typically yield low ^{3}He/^{4}He$_m$ and, if unaccounted for, it leads to an over-correction of the magmatic component that reduces the apparent cosmogenic ^{3}He concentration and lowers the apparent exposure age (Dunai and Wijbrans, 2000). To avoid contamination by implanted ^{4}He from the matrix olivine separates were etched in a second step to remove the outer part of all crystals (see Section 3.2). The cosmogenic ^{3}He concentrations of the double-etched samples calculated with equation (1) are up to ~10% higher than the single-etched samples (Fig. 3). Thus chemical etching may prove to be a valid alternative to using small mineral fractions (Williams et al., 2005) to date basaltic flows with cosmogenic ^{3}He in cases where the amount of *in situ* produced radiogenic ^{4}He is small.

The effect of *in situ* and implanted radiogenic ^{4}He on cosmogenic ^{3}He exposure ages of uneroded lavas can be quantified by calculating the so called *R*-factor (Blard and Farley, 2008):

$$R = 1 - \frac{P_{4\ \mathrm{mean}}}{P_{3\ \mathrm{mean}}} \times \left(\frac{^3\mathrm{He}}{^4\mathrm{He}}\right)_{cr} \quad (2)$$

P_{4mean} and P_{3mean} are the production rates of radiogenic ^{4}He and cosmogenic ^{3}He respectively (Blard and Farley, 2008). P_{4mean} is the sum of the *in situ* produced radiogenic ^{4}He with the production rate I_4 and the implanted radiogenic ^{4}He from the matrix with the

Table 3
Trace elements of whole rock basalts [ppm].

Sample name	Zn	Cu	Ni	Cr	V	Ba	Sc	Nb	Zr	Y	La	Ce	Nd	Sr	U	Rb	Th	Pb
CH1	138	55.9	100.1	141.1	230.7	220.6	27.2	24.5	127.7	25.9	14.3	37.8	21.3	451.5	0.3	6.7	2.0	2.2
CH5	130	64.6	96.1	146.8	249.8	209.6	30.1	27.1	142.2	26.1	15.7	40.5	22.0	479.0	0.6	5.6	2.3	1.5
DC5	101	59.0	108.4	154.4	236.3	192.7	28.2	28.2	150.5	25.9	14.8	40.8	24.5	435.3	0.3	7.4	1.9	2.4
DC1	111	61.7	98.8	170.8	263.2	220.6	33.3	22.1	117.9	23.0	12.5	33.6	21.7	430.6	0.3	6.0	2.1	1.2
PAL-B1	126	37.3	46.1	32.1	303.3	270.6	32.5	38.2	219.3	31.6	24.3	59.3	32.0	396.7	0.3	10.0	3.3	1.6
PAL-B5	146	34.4	46.4	34.6	297.8	281.6	33.2	39.5	223.4	29.9	23.1	55.4	29.0	407.9	0.4	11.9	3.4	1.6
SWRH1	124	55.1	109.2	154.1	236.6	181.5	26.1	26.2	133.3	26.4	16.5	43.1	23.7	451.2	0.4	8.8	2.0	1.0
SWRH4	140	61.4	99.3	146.0	262.5	206.2	28.3	28.2	145.1	30.6	20.1	48.3	26.5	507.7	0.6	4.1	2.2	1.4
UV1	99.0	18.8	9.3	10.0	121.3	424.2	15.9	58.7	277.8	34.1	36.7	78.0	38.0	649.4	1.7	25.5	4.4	3.1
UV2	97.3	16.8	13.4	12.0	126.5	404.1	16.2	58.5	278.4	33.4	38.9	79.2	39.3	664.3	1.2	24.3	4.5	3.1

Table 4
Major elements of whole rock basalts [oxide %].

Sample name	SiO_2	Al_2O_3	Fe_2O_3	MgO	CaO	Na_2O	K_2O	TiO_2	MnO	P_2O_5	LOI	Total
CH-1	45.75	16.98	11.55	6.18	10.68	2.45	0.39	2.24	0.19	0.83	2.25	99.48
CH-5	45.14	16.95	12.21	6.18	10.19	2.11	0.36	2.40	0.18	1.15	2.50	99.37
DC-1	46.77	16.44	13.17	4.76	7.51	2.79	1.01	2.72	0.19	1.39	3.01	99.76
DC-5	51.17	19.57	7.87	2.15	8.05	3.99	1.41	1.70	0.14	1.22	2.70	99.97
PAL-B1	48.15	16.39	12.98	4.87	8.14	2.98	0.97	2.63	0.19	0.92	1.83	100.04
PAL-B5	42.31	15.97	12.90	6.56	9.53	1.86	0.38	2.37	0.18	2.73	2.39	97.19
SWRH-1	47.04	15.96	11.99	6.63	10.04	2.45	0.48	2.34	0.18	0.86	1.72	99.69
SWRH-4	46.43	15.51	12.40	5.99	9.97	2.29	0.37	2.48	0.18	1.23	2.72	99.58
UV-1	50.48	18.34	7.92	2.03	7.94	3.87	1.42	1.71	0.13	1.26	2.43	97.52
UV-2	44.62	16.18	11.31	6.70	10.99	2.17	0.37	2.06	0.16	0.98	1.89	97.43

production rate M_4 (for calculation details see Blard and Farley, 2008). P_{4mean} depends on the mean stopping distance of the produced radiogenic ^{4}He ($S \sim 20\ \mu m$) and the diameter of the analysed grain (D):

$$P_4 = I_4 \times \left[1 - 1.5 \times (S/D) + 0.5 \times (S/D)^3\right] + M_4 \times \left[1.5 \times (S/D) - 0.5 \times (S/D)^3\right] \quad (3)$$

R-factors usually range between 0 and 1, where values approaching 1 reflect no need for radiogenic correction.

To calculate the *R*-factor of the Ascension lavas we have used U and Th partition coefficients of 4% and 3% for basalt-pyroxene, and 3% and 2% for basalt-olivine (see Blard and Farley, 2008 and refs. therein). For grain sizes of 250–500 μm *R*-factors range between 0.955 ± 0.015 for the CH, DC, and PalB flows and 0.93 ± 0.03 for SWRH. The *R*-factor for the double-etched samples was calculated assuming the P_{4mean} reflected the *in situ* produced radiogenic ^{4}He only (I_4). The double-etched samples have *R*-factors >0.98. The *R* factor for UV samples is 0.805 ± 0.05 for grain sizes between 250 and 500 μm. Note, that etching would have increased the *R* factor to ~0.95. To correct for radiogenic ^{4}He exposure ages calculated using equation (1) have to be divided by *R*. Age differences between those with a magmatic correction only and the radiogenic correction are about 5% for single-etched olivines and about 1% for double-etched olivines for DC, CH, SWRH, and PalB. The radiogenic corrected exposure ages of pyroxene are 4–6% higher. As expected from the low *R*-factor the radiogenic correction of UV samples is up to 24%.

Olivine samples $CH4_{se}$, $CH5_{de}$, $SWRH1_{de}$, and $SWRH4_{de}$ were contaminated with ^{4}He-rich material during sample processing. By modifying equation (1) we calculate the cosmogenic ^{3}He assuming that all the non-cosmogenic He is radiogenic (i.e., no magmatic He) (Williams et al., 2005):

$$^3He_{cos} = {}^4He_m \times ({}^3He/{}^4He_m - {}^3He/{}^4He_{rad}) \quad (4)$$

where $^3He/^4He_{rad}$ is the radiogenic He ratio. We have assumed a radiogenic ratio of 0.01 R_A (where R_A is the air ratio 1.38×10^{-6}) in all calculations. This ratio is dependant on local variation in Li concentrations and can vary substantially (Pepin and Porcelli, 2002 and refs. therein). However, varying $^3He/^4He_{rad}$ from 0.1 to 0.001 produces less than 3% variation in exposure age. This is well within the analytical uncertainty and does impact significantly the accuracy of the exposure ages. Exposure ages of $CH4_{se}$ and $CH5_{de}$ calculated via Eq. (4) are equal to other CH samples within uncertainty. This gives us confidence in the alternative correction method.

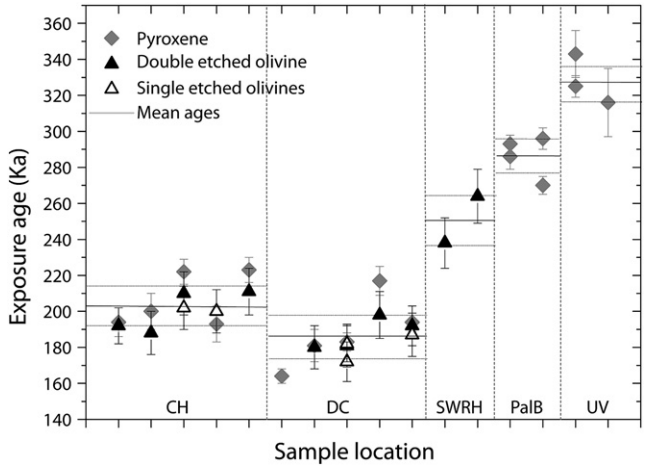

Fig. 3. Compilation of ^{3}He exposure age of olivine and pyroxene-phenocrysts from Ascension Island basalts.

4.2. Helium-3 exposure ages and implications for the evolution of Ascension Island

Model exposure ages of all flows are presented in Table 2 and plotted in Fig. 3. We use the long-term sea level high latitude (SLHL) production rate of 103 ± 4 atoms/g/yr for olivines measured by Dunai (2001). Several studies yielded undistinguishable cosmogenic ^{3}He concentrations in cogenetic olivine and pyroxene (e.g., Ackert et al., 2003; Blard et al., 2005) and modelled production rates for olivine and pyroxene (Masarik and Reedy, 1996) are equal within <4% using our sample chemistry (See Background dataset). Therefore we use the same SLHL for olivine and pyroxene. Local ^{3}He production rates are corrected for time-integrated magnetic field variations (Dunai, 2001) (correction factor 1.18). Topographic shielding for all sampling sites is <0.5 % and was therefore not corrected for. Assuming an average rock density of 2.2 g/cm^3 (based on a basalt density of 2.8 g/cm^3 and an observed vesicularity of 20%) a self-shielding of about 1.5% was calculated using an average sampling depth of 2.5 cm and an attenuation length of 170 ± 10 g/cm^2 for ^{3}He at low latitude (Gosse and Phillips, 2001; Kurz, 1986). Minshull et al. (2003) calculated a mean subsidence on Ascension Island of about 21 m/100 kyr for the last 2.5 Myr. Therefore our sample sites have subsided only 40–70 m. For such small altitude ranges, changes in production rates are linear. Assuming a constant subsidence rate, productions rate are corrected by ~3%.

The average ages of the flows are UV: 328 ± 11 ka, PalB: 286 ± 10 ka, SWRH: 251 ± 13 ka, CH: 203 ± 11 ka, and DC: 186 ± 13 ka (Fig. 3) whereas given uncertainties are the 1σ standard deviation of all samples. The exposure ages of cogenetic pyroxene and olivine agree in most cases to within <5%. Exposure ages of mineral separates from the same location mostly agree within 1σ uncertainty (Fig. 3). Judging from the concordance of ages (Table 2) it appears likely that the sampled flow tops are largely intact because locally variable erosion or intermittent ash cover tends to produce a scatter in exposure ages. Consequently they can be used

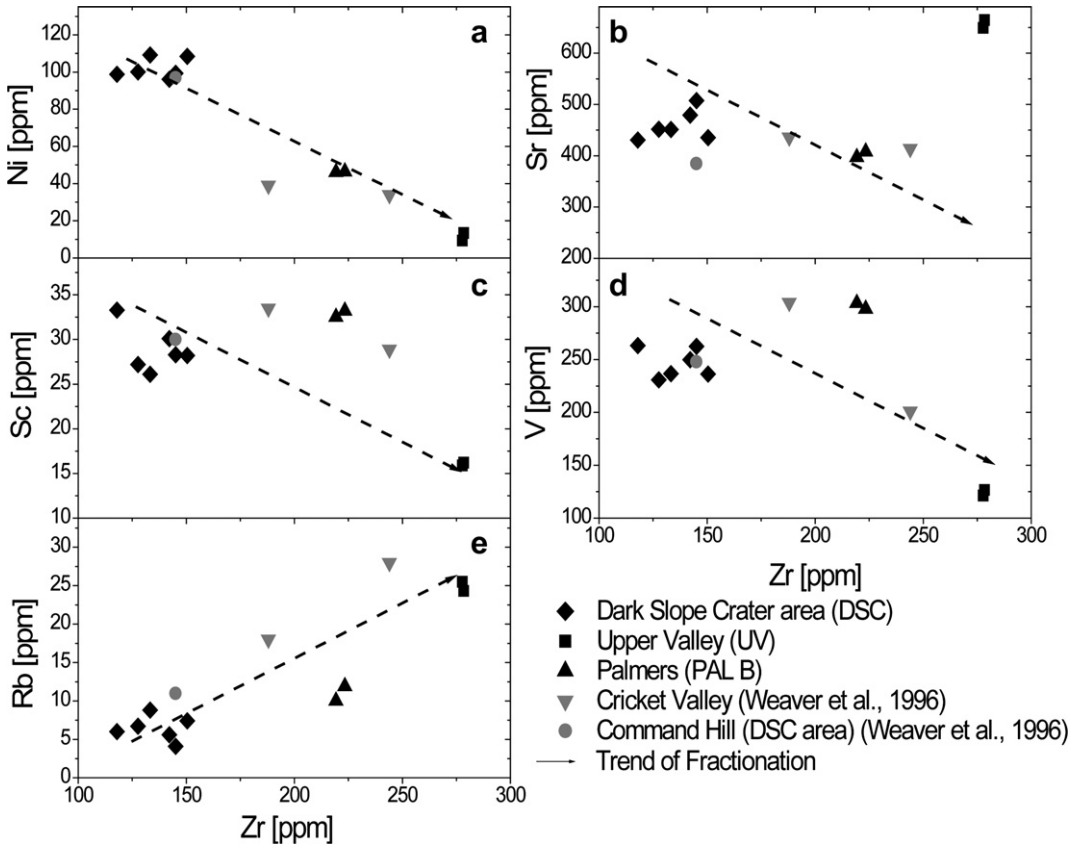

Fig. 4. a-e: Trace elements clearly show that CH, DC and SWRH belong to the same magma suite (DSC area black diamonds) but are different from PalB (black triangles) and UV (black squares). Comparing ages and geochemical signals of the different basalt suites it becomes clear that the different magma types could not be evolved from each other due to fractional crystallisation (arrows).

to place age constraints on the late Quaternary evolution on Ascension Island.

High-Zr/Nb hawaiite basalt flows between Cricket Valley, Palmers and Mountain Red Hill have K-Ar ages of 470–200 ka (Harris et al., 1982). The ^{3}He exposure age of 286 ± 10 ka of the PalB flow falls well into this range. Because this flow is one of the last high-Zr/Nb basalts to be erupted (suggestion from field observation) it is likely that this period of volcanism did not extend much past this time. At the end of this eruptive phase the high-Ni/Zr lavas appear to be erupted in the Dark Slope Crater area (DSC). On the basis of trace element compositions these basalts seem to have a different source as their trace element evolution cannot be explained by fractional crystallisation from the high-Zr/Nb basalts (Fig. 4a–e). The ^{3}He exposure ages of the CH, DC and SWRH flows indicate that the eruption of basalts in the DSC area lasted for at least 70 kyr, occurring between 251 ka and 186 ka. As surface

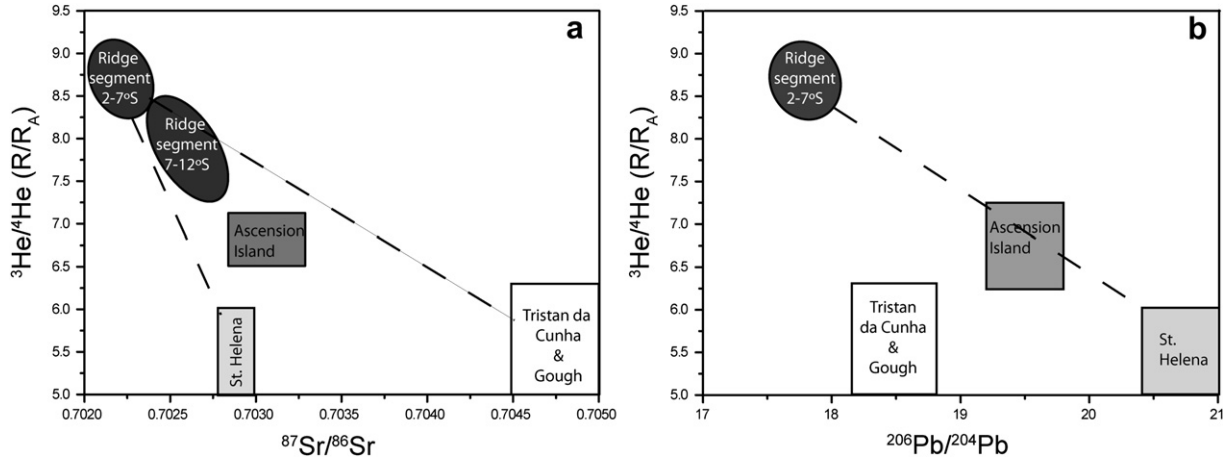

Fig. 5. a and b: Combining magmatic ^{3}He/^{4}He ratios from this work with Sr and Pb isotope determinations by Harris et al., (1982) it appears that the Ascension Island basalts lie on a mixing line between depleted mantle, sampled by MORB from 2 to 8°S, and the HIMU-type mantle that characterises basalts from St. Helena. There is little need to invoke a contribution from the enriched mantle that is prevalent further South in the Atlantic Ocean, e.g., Tristan da Cunha and Gough. Data for St. Helena, Tristan da Cunha and Gough are from (Chaffey et al., 1989; Cohen and O'Nions, 1982; Graham et al., 1992a; Kurz et al., 1982; LeRoex et al., 1990; Sun, 1980).

exposure dating only provides the age of the last basalts to be erupted in any given volcanic field it is not possible to tell if the eruption of the high-Ni/Zr basalts overlapped with the high-Zr/Nb basalts. For both basalt types the new data are in agreement with the relative geochronology of Weaver et al. (1996).

The intermediate Zr/Nb lava-type on the other hand, represented by the UV flow, is much older than was previously assumed (Weaver et al., 1996). The ^{3}He exposure ages of the UV flow (328 ± 11 ka) even predates the PalB flow which was assumed to belong to the oldest mafic lavas. Based on the geochemical signature the high-Zr/Nb lava could not be evolved from the intermediate Zr/Nb lava due to fractionation (Fig. 4a–e). Furthermore, the new ^{3}He exposure ages of the Ascension Island basalts overlap within 2σ uncertainties. Therefore, it is likely that magma chambers containing different types of magma coexisted beneath Ascension Island. This contradicts the assumption, based on field evidence and K–Ar chronology, that the volcanism occurred in temporally-discrete episodes (Weaver et al., 1996).

4.3. Helium isotope constraints on the origin of Ascension Island

There is little consensus on the ultimate source of the anomalous mantle melting beneath Ascension Island and the adjacent Mid-Atlantic Ridge (MAR). It has been argued that the formation of Ascension Island is related to tectonic adjustments involving rift jumps and rift migration caused by a mantle plume (Hanan et al., 1986). Brozena (1986) suggested a scenario where the material from a weak mantle plume is channelled through the MAR and stopped by the Ascension Fracture Zone to form the seamounts and islands from the excess melt. During the transport of the melt, material from the plume would be mixed with material from the MORB source obliterating the plume signature.

Radiogenic isotopes and trace element geochemistry of basalts cannot be used to distinguish shallow melt anomalies from deep-sourced material. Helium isotopes are frequently used to identify deep mantle-derived plumes (e.g., Stuart et al., 2003 and refs. therein). Here we use the helium isotope composition of the crush-released magmatic volatiles to test the prevailing hypothesis. The magmatic ^{3}He/^{4}He ratio of the Ascension Island basalts ranges between 6.3 and 7.3 R_A. There is no significant variation between the three basalt types within analytical uncertainty, and the average ^{3}He/^{4}He is 6.8 ± 0.4 R_A. The ^{3}He/^{4}He range is slightly lower than that measured in basalts erupted along the Mid-Atlantic Ridge segment between 2–7 °S (8.6 ± 0.3 R_A, $n = 6$) and 7–12 °S (7.8 ± 0.2 R_A, $n = 7$) (Graham et al., 1992b) (Fig. 5). But it is slightly higher than the ^{3}He/^{4}He of basalts from the nearest ocean islands, i.e., St Helena, Tristan da Cunha, and Gough which ranges between 5 and 6 R_A (Graham et al., 1992b and refs. therein). Contamination by shallow-level assimilation of radiogenic He-bearing crust (e.g., Hilton et al., 1995) is unlikely as the ^{3}He/^{4}He ratio of cogenetic olivine and pyroxene are indistinguishable. Release of post-eruptive radiogenic ^{4}He during crushing would decrease ^{3}He/^{4}He in samples with low magmatic He concentrations. However, the SUERC crush procedure does not release *in situ* radiogenic He from 61 Ma olivines (Stuart et al., 2003) so we consider it unlikely to have affected sub-1 Ma phenocrysts. This is supported by the apparent constancy of crush ^{3}He/^{4}He values (Table 2).

Consequently we believe that the data support an origin for Ascension Islands in a mantle source with a lower time-integrated ^{3}He/(U + Th) ratio than MORB-source mantle. Although it does not provide a constraint on the type of enriched mantle that is melting beneath Ascension Island, it rules out an origin in a deep-sourced mantle plume that is characterised by high ^{3}He/^{4}He ratios. To investigate the source of enriched mantle beneath Ascension Island our He isotope data are combined with published Sr and Pb isotope data from the same basalt types from similar areas measured by Harris et al., (1982) (Fig. 5a and b). From Fig. 5 it appears that the Ascension Island basalts lie on a mixing line between depleted mantle, sampled by MORB from 2 to 8°S MAR, and the HIMU-type mantle that characterises basalts from St. Helena. Importantly there is little need to invoke a contribution from the enriched mantle that is prevalent further south in the Atlantic Ocean, e.g., Tristan da Cunha and Gough. The widespread distribution of the HIMU-type mantle in the South Atlantic Ocean is difficult to explain in the classical view of a plume sourced in the deep mantle. The proximity of these HIMU-type hotspots to the MAR implies a connection with the mantle upwelling at the ridge. Possibly they originate as enriched mantle heterogeneities that melt as they upwell into the sub-ridge melting zone.

5. Conclusions

We have analysed the helium isotopic abundances in phenocrysts from Ascension Island basalts for surface exposure dating. The ^{3}He/^{4}He ratio of trapped gases and the major and trace element composition were used to determine the geochemical provenance of the mantle source. We demonstrate that significant etching of samples (mass loss of ~30%) improves the accuracy of calculated cosmogenic ^{3}He concentration by eliminating implanted radiogenic ^{4}He. Three basalt suites on Ascension Island, distinguished by their trace element ratios (Weaver et al., 1996) and geographic location, have average ^{3}He exposure ages of 328 ± 11 ka and 286 ± 10 for UV (intermediate Zr/Nb) and PalB (high-Zr/Nb), and 186 ± 13 ka, 203 ± 11 ka, and 251 ± 13 ka for the Dark Slope Crater area (high Ni/Zr), respectively. The eruption of the intermediate Zr/Nb basalts (UV) appears to have occurred earlier than the high-Zr/Nb (PalB) type contrary to the stratigraphic evidence of Weaver et al. (1996). Based on the new ages and literature data we conclude that the coexistence of multiple magma chambers with different geochemical signatures is very likely beneath Ascension Island. The magmatic ^{3}He/^{4}He (6.8 ± 0.4 R_A) is slightly lower than in MORB from the adjacent Mid-Atlantic Ridge, but higher than in regional hotspot basalts. Combining the He isotope data with published Sr and Pb isotopes it appears that the Ascension Island basalts can most simply be explained as a mix of normal depleted mantle with HIMU mantle source that is sampled by the St Helena hotspot.

Acknowledgements

We wish to thank Elaine McDougall for help with the chemical mineral separation and etching procedure, Roel van Elsas for mineral seperation and Jurgen Foeken in the noble gas isotope laboratory. We thank Chris Place for helping us displaying the bathymetric data. We are grateful to M. Moreira and P.-H. Blard for their helpful comments and suggestions to improve the manuscript.

Editorial handling by: F. Stuart

Appendix. Supplementary data

Supplementary data associated with this article can be found in the online version, at 10.1016/j.quageo.2009.09.003.

References

Ackert, R.P., Singer, B.S., Guillou, H., Kaplan, M.R., Kurz, M.D., 2003. Long-term cosmogenic ^{3}He production rates from ^{40}Ar/^{39}Ar and K–Ar dated Patagonian lava flows at 47°S. Earth and Planetary Science Letters 210, 119–136.

Blard, P.-H., Farley, K.A., 2008. The influence of radiogenic ^{4}He on cosmogenic ^{3}He determinations in volcanic olivine and pyroxene. Earth and Planetary Science Letters 276, 20–29.

Blard, P.-H., et al., 2005. Fossil cosmogenic ^{3}He record from K–Ar dated basaltic flows of Mount Etna volcano (Sicily, 38°N): evaluation of a new paleoaltimeter. Earth and Planetary Science Letters 236, 613–631.

Blard, P.-H., et al., 2006. Cosmogenic ^{3}He production rates revisited from evidences of grain size dependent release of matrix-sited helium. Earth and Planetary Science Letters 247, 222–234.

Bourdon, E., Hemond, C., 2001. Looking for the "missing endmember" in South Atlantic Ocean mantel around Ascension Island. Mineralogy and Petrology 71, 127–138.

Brozena, J.M., 1986. Temporal and Spatial Variability of Seafloor Spreading Processes in the Northern South Atlantic. Journal of Geophysical Research 91 (B1), 497–510.

Chaffey, D.J., Cliff, R.A., Wilson, B.M., 1989. Characterization of the St. Helena magma source. In: Norry, A.D.S.a.M.J. (Ed.), Magmatism in Ocean Basins. Geol. Soc. Spec. Publ.

Cohen, R.S., O'Nions, R.K., 1982. Identification of recycled continental material in the mantle from Sr, Nd and Pb isotope investigations. Earth and Planetary Science Letters 61, 73–84.

Dunai, T.J., 2001. Influence of secular variation of the geomagnetic field on production rates of in situ produced cosmogenic nuclides. Earth and Planetary Science Letters 193, 197–212.

Dunai, T.J., Wijbrans, J.R., 2000. Long-term cosmogenic ^{3}He production rates (152 ka–1.35 Ma) from ^{40}Ar/^{39}Ar dated basalt flows at 29°N latitude. Earth and Planetary Science Letters 176, 147–156.

Foeken, J.P.T., Day, S., Stuart, F.M., 2009. Cosmogenic ^{3}He exposure dating of the Quaternary basalts from Fogo, Cape Verdes: Implications for rift zone and magmatic reorganization. Quaternary Geochronology 4, 37–49.

Foeken, J.P.T., Stuart, F.M., Dobson, K.J., Persano, C., Vilbert, D., 2006. A diode laser system for heating minerals for (U–Th)/He chronometry. Geochemistry, Geophysics, Geosystems 7 (4), 1–9.

Gosse, J.C., Phillips, F.M., 2001. Terrestrial in situ cosmogenic nuclides: Theory and application. Quaternary Science Reviews 20, 1475–1560.

Graham, D.W., Humphris, S.E., Jenkins, W.J., Kurz, M.D., 1992a. Helium isotope geochemistry of some volcanic rocks from Saint Helena. Earth and Planetary Science Letters 110, 121–131.

Graham, D.W., et al., 1992b. Helium isotope geochemistry of mid-ocean ridge basalts from the South Atlantic. Earth and Planetary Science Letters 110, 113–147.

Hanan, B.B., Kingsley, R.H., Schilling, J.-G., 1986. Pb isotope evidence in the South Atlantic from migrating ridge-hotspot interactions. Nature 322, 137–144.

Harris, C., Bell, J.D., Atkins, F.B., 1982. Isotopic composition of lead amd strontium in lavas and coars-grained bolcks from Ascension Island, South Atlantic. Earth and Planetary Science Letters 60, 79–85.

Hilton, D.R., Barling, J., Wheller, G.E., 1995. Effect of shallow-level contamination on helium isotope systematics of ocean-island lavas. Nature 373, 330–333.

Kar, A., Weaver, B., Davidson, J., Colucci, M., 1998. Origin of Differentiated Volcanic and Plutonic Rocks fromAscension Island, South Atlantic Ocean. Journal of Petrology 39 (5), 1009–1024.

Klingelhoefer, F., Minshull, T.A., Blackman, D.K., Harben, P., Childers, V., 2001. Crustal structure of Ascension Island from wide-angle seismic data: implication for thr formation of near-ridge volcanic islands. Earth and Planetary Science Letters 190, 41–56.

Kurz, M.D., 1986. In-situ production of terrestrial cosmogenic helium and some applications to geochronology. Geochimica et Cosmochimica Acta 50 (12), 2855–2862.

Kurz, M.D., Colodner, D., Trull, T.W., Moore, R.B., O'Brien, K., 1990. Cosmic ray exposure dating with in situ produced cosmogenic ^{3}He: results from young Hawaiian lava flows. Earth and Planetary Science Letters 97, 177–189.

Kurz, M.D., Jenkins, W.J., Hart, S.R., 1982. Helium isotopic systematics of oceanic islands and mantle heterogeneity. Nature 297, 43–46.

Laughlin, A.W., Poths, J., Healey, H.A., Reneau, S., WoldeGabriel, G., 1994. Dating of Quaternary basalts using the cosmogenic ^{3}He and ^{14}C methods with implications for excess ^{40}Ar. Geology 22, 135–138.

LeRoex, A.P., Cliff, R.A., Adair, B.J.I., 1990. Tristan da Cunha, South Atlantic: geochemistry and Petrogenesis of a Basanite-Phonolite Lava Series. Journal of Petrology 31, 779–812.

Masarik, J., Reedy, R.C., 1996. Monte Carlo simulation of *in-situ*-produced cosmogenic nuclides. Radiocarbon 38 (1), 163–164.

Minshull, T.A., Bruguier, N.J., Brozena, J.M., 1998. Ridge-plume interactions or mantle heterogeneity near Ascension Island? Geology 26 (2), 115–118.

Minshull, T.A., Ishizuka, O., Mitchell, N.C. and Evangelidis, C., 2003. Vertical motion and Lithosphere rheology at Ascension Island. AGU abstract, V11B-06.

Nielson, D.L., Sibbett, B.S., 1996. Geology of Ascension Island, South Atlantic Ocean. Geothermics 25 (4/5), 427–448.

Nielson, D.L., Stiger, S.G., 1996. Drilling and evaluation of Ascension #1, a geothermal exploration well on Ascension Island, South Atlantic Ocean. Geothermics 25 (4/5), 543–560.

Pepin, R.O., Porcelli, D., 2002. Origin of Noble Gases in Terrestrial Planets. In: Reviews in Mineralogy and Geochemistry, vol. 47. Mineralogical Society of America, pp. 191–246.

Staudacher, T., Allegre, C.J., 1993. Ages of the second caldera of Piton de la Fournaise volcano (Reunion) determined by cosmic ray produces ^{3}He and ^{21}Ne. Earth and Planetary Science Letters 119, 395–404.

Stuart, F.M., Lass-Evans, S., Fitton, J.G., Ellam, R.M., 2003. Extreme ^{3}He/^{4}He in picritic basalts from Baffin Island: role of a mixed reservoir in mantle plumes. Nature 424, 57–59.

Sun, S.-S., 1980. Lead isotope study of young volcanic rocks from mid-ocean ridges, ocean islands and island arcs. Philosophical Transactions of the Royal Society of London. Series A 297, 409–445.

Weaver, B., Kar, A., Davidson, J., Colucci, M., 1996. Geochemical characteristics of volcanic rocks from Ascension Island, South Atlantic Ocean. Geothermics 25 (4/5), 449–470.

Williams, A.J., Stuart, F.M., Day, S.J., Phillips, W.M., 2005. Using pyroxene microphenocrysts to determine cosmogenic ^{3}He concentrations in old volcanic rocks: an example of landscape development in central Gran Canaria. Quaternary Science Reviews 24, 211–222.